

# An Anthropomorphic Software Breast Phantom for Tomosynthesis Simulation: Power Spectrum Analysis of Phantom Projections

Predrag R. Bakic<sup>1</sup>, Beverly Lau<sup>2</sup>, Ann-Katherine Carton<sup>1</sup>, Ingrid Reiser<sup>2</sup>, Andrew D.A. Maidment<sup>1</sup>, and Robert M. Nishikawa<sup>2</sup>

<sup>1</sup> University of Pennsylvania, Dept. of Radiology, Philadelphia, PA 19104 ,

<sup>2</sup> University of Chicago, Dept. of Radiology, Chicago, IL 60637

{Predrag.Bakic,Ann-Katherine.Carton,

Andrew.Maidment}@uphs.upenn.edu

{Beverly,IReiser,R-Nishikawa}@uchicago.edu

**Abstract.** We have performed spectral analysis of simulated tomosynthesis projections generated using an anthropomorphic software breast phantom. Twenty phantoms were generated: ten 450 ml phantoms with 40% glandular fraction and ten 1500 ml phantoms with 20% glandular fraction. Simulated mammographic compression and acquisition was performed using monoenergetic ray-tracing. ROIs were extracted and the modulus-squared 2D FFT was applied to each ROI to obtain periodograms. Radially-averaged periodograms were compared between phantom and clinical images. We observed a good agreement between the spectral power law exponents ( $\beta$ ) calculated from phantom projections and clinical images.

**Keywords:** breast anthropomorphic phantom, digital breast tomosynthesis, power law, power spectrum.

## 1 Introduction

Clinical validation of novel breast imaging systems is largely unfeasible today as it requires long and expensive clinical trials. On the other hand, physical characteristics of imaging systems such as the MTF, NNPS and NEQ, do not necessarily predict the behavior of the human observer scrutinizing complex mammographic backgrounds and do not take into account clinical processing or display. In an alternative approach, a voxelized anthropomorphic software breast phantom has been developed for use in pre-clinical validation of breast imaging modalities. The phantom realistically simulates the spatial distribution of adipose and fibroglandular tissues with known ground truth in simulated images. Projections of simulated tissue structures generate realistic parenchymal pattern, called anatomical noise. The anatomical noise is known to affect visibility of breast lesions. [1].

A frequently used descriptor of the anatomical noise is the power law exponent ( $\beta$ ) of the radially-averaged periodogram. A periodogram is the modulus-squared 2D discrete Fourier transform of a region of interest (ROI). Burgess *et al.* [2] demonstrated

that periodograms of digitized clinical mammograms follow a power law,  $P(f) = B/f^\beta$ . They performed spectral analysis of  $46 \times 46$  mm regions in 213 mammograms and calculated the average power law exponent  $\beta$  to be 2.83 with a standard deviation  $\sigma=0.35$ . Engstrom *et al.* [3] analyzed the periodograms from tomosynthesis projection views and reconstructed images. Using  $12.8 \times 12.8$  mm regions in 55 cases, they found the mean  $\beta$  to be 3.06 ( $\sigma=0.21$ ) in the projection view images and 2.87 ( $\sigma=0.24$ ) in the reconstructed images. In this paper we report results of estimating  $\beta$  in simulated tomosynthesis images of a software breast phantom.

## 2 Materials and Methods

We used an anthropomorphic breast phantom described by Bakic *et al.* [4,5], designed based upon the analysis of a large number of clinical breast images and histological slides. The phantom simulates the ellipsoidal shape of the breast outline. The phantom interior includes regions of predominantly adipose and predominantly fibroglandular tissues, and internal tissue structures (adipose compartments and Cooper's ligaments), as illustrated in Fig. 1. The design of the phantom is flexible to cover anatomical variations in breast composition and size.

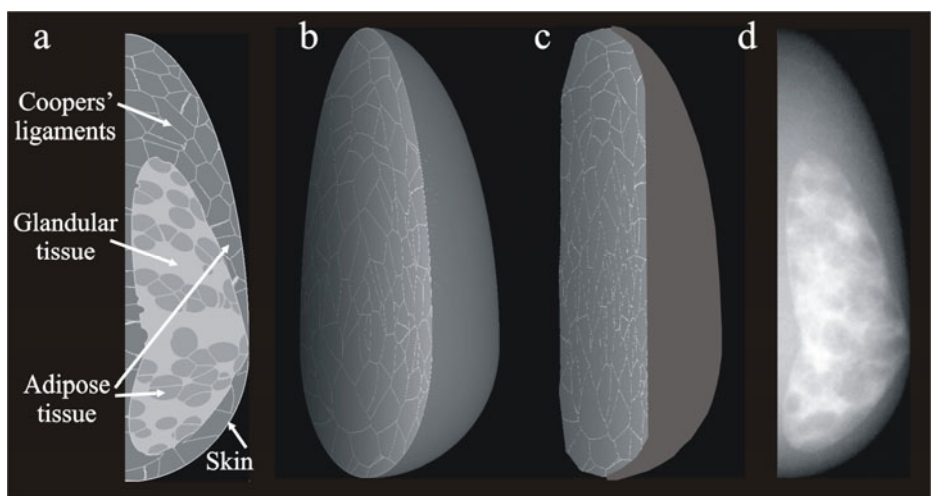


**Fig. 1.** (a) Orthogonal slice through a software breast phantom. Phantom outlines prior (b) and after (c) simulated mammographic compression. (d) Simulated x-ray projection image of the phantom.

For this study, we used ten 450 ml phantoms with 5 cm compressed thickness and ten 1500 ml, 7.5-cm thick phantoms. The 450 ml phantoms were generated with 40 percent by volume of fibroglandular tissue, while the 1500 ml phantoms were generated with 20 percent by volume of fibroglandular tissue. These glandularities were chosen in light of recent studies that have revealed that 95% of women have breast glandularity below 45% [6].

We simulated mammographic breast compression using a finite element model of tissue deformation. Simulated tomosynthesis projection images of the breast phantom were acquired using a monoenergetic x-ray beam without scatter or quantum noise by a detector which did not introduce any noise or blurring. Ray-tracing was used to calculate the x-ray attenuation through the phantom. The detector pixel resolution was matched with the voxel resolution of the phantom (500 micron). The acquisition geometry included 11 views over a 50-degree arc, with the center of rotation 15 cm above the breast [7].

$\beta$  values were calculated on the tomosynthesis projection images using the method described by Engstrom *et al.* [3]. For this study, we selected 32×32 mm ROIs that were completely contained within the projected phantom region. ROIs were allowed to overlap by 50%; this is consistent with previous reports in the literature [2]. To reduce spectral leakage, we used a radial Hanning window on the mean-subtracted ROIs. The modulus-squared 2D FFT of each filtered ROI was calculated, and the obtained periodograms were each radially-averaged to reduce noise.  $\beta$  values were calculated as the slope of the linear portion of the log-log plot of the radially-averaged periodogram; these  $\beta$  values were evaluated from 0.15 to 0.7 cycles/mm.  $\beta$  values from all ROIs extracted from one breast and one projection view were averaged, and this average is denoted by  $\beta'_{\text{breast}}$ .  $\beta_{\text{breast}}$  indicates that the average was taken across one breast and all projection views.

### 3 Results

Fig. 2 shows examples of ROIs from simulated tomosynthesis phantom projections with corresponding periodograms and 1-D power spectra approximations (radially averaged periodograms).  $\beta$  values for individual ROIs in a single phantom projection image were found to range between 1.5 and 3.5. Fig. 3 shows  $\beta'_{\text{breast}}$  values as a function of tomosynthesis projection angle. Tables 1 and 2 show  $\beta_{\text{breast}}$  averaged over projection angles and averaged over breast phantoms. The average of  $\beta_{\text{breast}}$  over all the phantoms of the same size were 2.65 ( $\sigma=0.318$ ) for 450ml phantoms and 2.62 ( $\sigma=0.412$ ) for 1500ml phantoms. Note that  $\sigma$  is the average standard deviation of  $\beta$  values found in a breast.

**Table 1.** A summary of  $\beta_{\text{breast}}$  values and standard deviations for ten 450 ml phantoms and ten 1500 ml analyzed breast phantoms. Mean values and standard deviation were calculated for all ROIs from all projection views for each phantom.

<i>450 ml phantoms</i>			<i>1500 ml phantoms</i>		
<i>Phantom ID</i>	$\beta_{\text{breast}}$	$\sigma_{\beta}$	<i>Phantom ID</i>	$\beta_{\text{breast}}$	$\sigma_{\beta}$
B1	2.604	0.305	DD1	2.648	0.400
B2	2.640	0.316	DD2	2.654	0.463
B3	2.621	0.318	DD3	2.618	0.430
B4	2.673	0.255	DD4	2.569	0.380
B5	2.664	0.360	DD5	2.650	0.347
B6	2.665	0.282	DD6	2.544	0.395
B7	2.693	0.355	DD7	2.603	0.369
B8	2.703	0.356	DD8	2.585	0.449
B9	2.651	0.289	DD9	2.582	0.434
B10	2.626	0.348	DD10	2.765	0.451
<i>Average</i>	2.654	0.318	<i>Average</i>	2.622	0.412

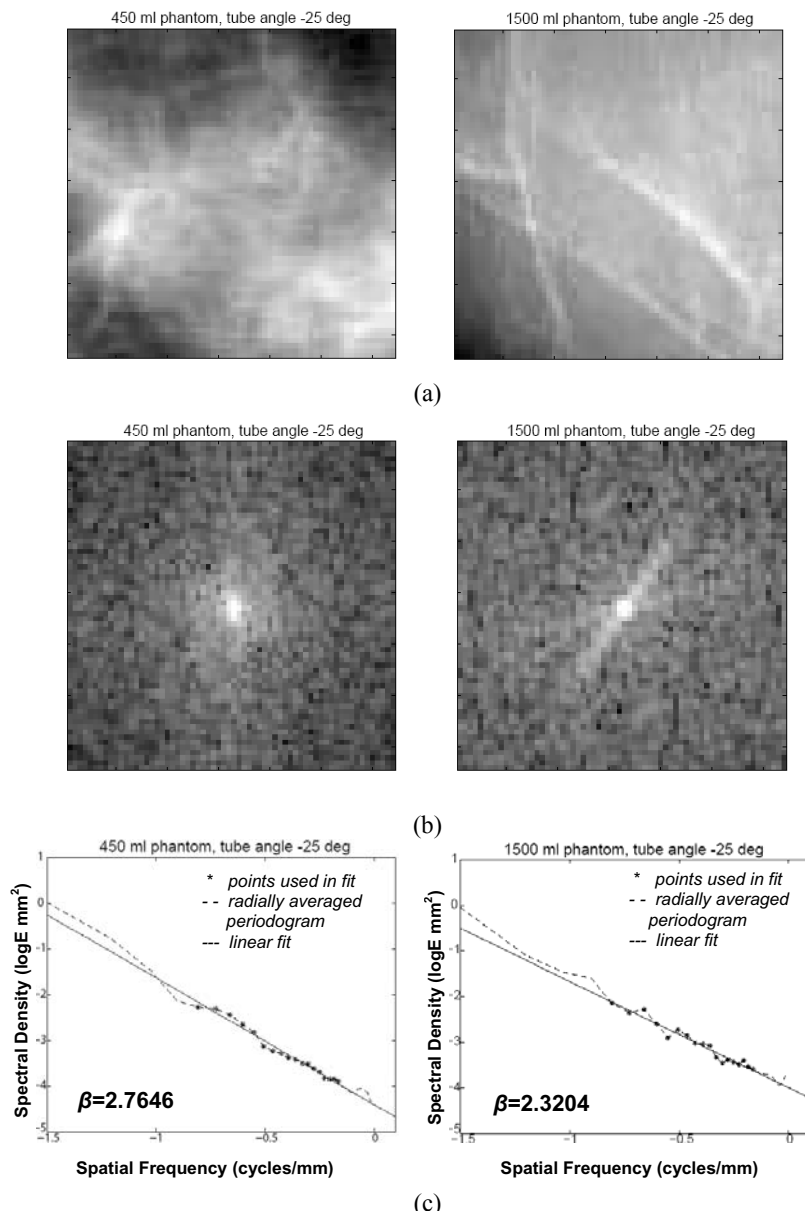


**Fig. 2.** Estimation of  $\beta$  values. (a) 32 mm  $\times$  32 mm ROIs from phantom projections. (b) Corresponding periodograms. (c) 1-D power spectra for a 450 ml (left column) and a 1500 ml phantom (right column).

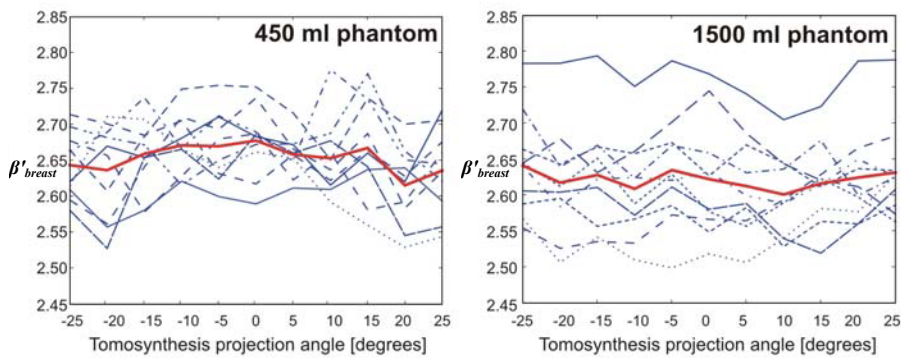


**Fig. 3.** Dependence of  $\beta'$ <sub>breast</sub> values on the tomosynthesis projection angle for ten 450 ml software breast phantoms (left) and ten 1500 ml phantoms (right). Blue (dashed or solid) lines are  $\beta'$ <sub>breast</sub> values for individual phantoms, and red (bold) lines are  $\beta'$ <sub>breast</sub> values averaged over all phantoms of the same size.

**Table 2.** Average  $\beta'$ <sub>breast</sub> values for projection views averaged over ten 450 ml phantoms and ten 1500 ml analyzed phantoms. Standard deviation was calculated across the  $\beta'$ <sub>breast</sub> values for ten phantoms at each tube angle.

Tube angle	450 ml phantoms		1500 ml phantoms	
	$\langle \beta'$ <sub>breast</sub> $\rangle$	$\sigma(\beta'$ <sub>breast</sub> )	$\langle \beta'$ <sub>breast</sub> $\rangle$	$\sigma(\beta'$ <sub>breast</sub> )
-25°	2.644	0.043	2.641	0.066
-20°	2.637	0.064	2.617	0.074
-15°	2.659	0.048	2.628	0.073
-10°	2.671	0.041	2.609	0.067
-5°	2.670	0.046	2.635	0.075
0°	2.678	0.046	2.622	0.078
5°	2.658	0.027	2.613	0.066
10°	2.653	0.050	2.601	0.054
15°	2.668	0.064	2.616	0.054
20°	2.616	0.050	2.625	0.064
25°	2.636	0.056	2.632	0.062

## 4 Discussion

The range of  $\beta$  values estimated from phantom projections (1.5-3.5) is consistent with the range reported in the literature (1.5-4.5) [3]. The average  $\beta$ <sub>breast</sub> values (2.65 for 450 ml phantoms and 2.62 for 1500 ml phantoms) are comparable with clinical measurements from digitized mammograms (average  $\beta$ <sub>breast</sub> = 2.83) [2] and tomosynthesis projection view images (average  $\beta$ <sub>breast</sub> = 3.06) [3]. The average  $\beta$ <sub>breast</sub> values from the phantom are slightly lower than those reported in the literature. This might be due to the fact that the  $\beta$ <sub>breast</sub> values reported in the literature were estimated from contralateral breast images of women with a known breast lesion; parenchymal properties of contralateral breasts

are known to be correlated with risk of cancer. The phantom images used in our study did not include any lesions nor did they simulate high-risk parenchymal patterns.

The tomosynthesis projection angle has almost no effect on the measurement of  $\beta'_{\text{breast}}$ . In this preliminary study of two groups of phantoms we did not observe a significant effect of the breast volume or glandularity on the estimated  $\beta'_{\text{breast}}$  values. Further analysis will include more groups of phantoms with different volume, thickness, and glandularity.

We identified limitations of our acquisition simulation approach. We have not used any quantum or detector noise and have not included scatter or detector blur. The inclusion of stochastic noise would affect the power spectrum at high frequencies (above approximately 1.0 cycles/mm [3]). The range of frequencies we have used to estimate  $\beta$  in this study will likely not be affected by the addition of quantum and detector noise. Scatter may increase the entire signal by a uniform amount with potentially a smaller increase at the edges of the image. Since we are using ROIs that do not encompass the entire image, we do not expect a large increase in the low frequency component of the approximated 1D power spectrum.

## 5 Conclusions

Power-law exponents calculated from simulated tomosynthesis projections through an anthropomorphic software breast phantom are comparable with clinically estimated values.

**Acknowledgments.** Funding for this research was sponsored in part by DOD BCRP predoctoral fellowship W81XWH-080-1-0353. The project described was supported in part by award R21 EB008801 from the National Institute of Biomedical Imaging and Bioengineering. The content is solely the responsibility of the authors and does not necessarily represent the official views of the National Institute of Biomedical Imaging and Bioengineering or the National Institutes of Health. RM Nishikawa is a shareholder in and receives royalties from Hologic, Inc. He is a member of the scientific advisory board of Dexela, Ltd. He is a consultant to Siemens Medical Solutions USA and Carestream Health, Inc.

## References

1. Burgess, A.E., Jacobson, F.L., Judy, P.F.: Human observer detection experiments with mammograms and power-law noise. *Medical physics* 28, 419–437 (2001)
2. Burgess, A.E.: Mammographic structure: data preparation and spatial statistics analysis. In: Proc. SPIE, vol. 3661, pp. 642–653 (1999)
3. Engstrom, E., Reiser, I., Nishikawa, R.: Comparison of power spectra for tomosynthesis projections and reconstructed images. *Medical Physics* 36, 1753–1758 (2009)
4. Bakic, P.R., Albert, M., Brzakovic, D., Maidment, A.D.A.: Mammogram synthesis using a 3D simulation. I. Breast tissue model and image acquisition simulation. *Medical Physics* 29, 2131–2139 (2002)

5. Zhang, C., Bakic, P.R., Maidment, A.D.A.: Development of an Anthropomorphic Breast Software Phantom Based on Region Growing Algorithm. In: Proc. SPIE, Visualization, Image-guided procedures, and Modeling, vol. 6918 (2008)
6. Wu, T., Moore, R., Rafferty, E., Kopans, D.: A comparison of reconstruction algorithms for breast tomosynthesis. Medical Physics 31, 2636–2647 (2004)
7. Yaffe, M.J., Boone, J.M., Packard, N., Alonzo-Proulx, O., Huang, S.Y., Peressotti, C.L., Al-Mayah, A., Brock, K.: The myth of the 50-50 breast. Medical Physics 36, 5437–5443 (2009)